

DOI: 10.1002/adma.200701607

Stress-Driven Surface Topography Evolution in Nanocrystalline Al Thin Films**

By Daniel S. Gianola, Christoph Eberl, Xuemei Cheng, and Kevin J. Hemker*

In their as-fabricated state, nanocrystalline (nc) materials, consisting of individual grains or crystallites with diameters less than 100 nm, are systems that exist far from equilibrium. The large volume fraction of grain boundaries (GB) present in these materials contains considerable excess free energy, which provides a large driving force for grain growth. Grain growth in nc materials has been reported to occur spontaneously^[1] and with relatively small thermal loads,^[2] but a surprisingly large number of nc materials exhibit remarkable thermal stability. The long-term stability of these materials is not fully understood and is an area that is receiving increased attention.^[3] Indeed, numerous synthesis techniques have been implemented to create nc materials that demonstrate unique optical, magnetic, electrical, and mechanical properties in comparison to their coarse-grained counterparts. Superior mechanical behavior, such as elevated strengths and improved fatigue resistance, has been reported^[4] and has fueled an intense desire to use these materials for structural applications.

Of particular interest in the current study is the fact that room-temperature stress-assisted grain growth has been shown to have a dramatic and dynamic effect on the deformation behavior in certain nc metals. Although this phenomenon has not been universally reported in nc materials, studies of Al,^[5] Cu,^[6] Co,^[7] Ni,^[8] and Fe^[9] have shown changes in hardness, strength, and ductility that are due to nanostructural evolution. These experiments report post-mortem deformation observations of grain growth, but direct in situ transmission electron microscopy (TEM) observations of localized grain coalescence and agglomeration have also been reported.^[10] The profound influence of stress-assisted grain growth in nc Al is described in detail in earlier work;^[5] briefly, two general classes of deformation behavior are measured. The

first is exhibited by nc metals that maintain a stable microstructure during deformation and show very strong but brittle behavior. In contrast, nominally identical specimens demonstrating microstructural evolution display intermediate strength and surprisingly large amounts of tensile ductility. Traditional driving forces for thermal grain growth (e.g., GB surface tension, surface energy minimization, inhomogeneously stored dislocations, elastic strain energy anisotropy) have been considered, but evidence to support these is limited. The inability to describe the characteristics of the grain growth in nc-Al freestanding thin films with traditional driving forces for grain growth and the observation of growth only in the highly deformed regions of the sample suggest that stress-assisted GB migration is the underlying cause of these phenomena.^[5] The level of impurities appears to be a key feature in distinguishing between nc materials that exhibit stress-assisted grain growth and those that do not. In particular, increasing the impurity content, by adjusting the vacuum base pressure during deposition, increases the nanostructural stability of nc-Al thin films.^[11] This provides the potential for using processing techniques with precise dopant control as a strategy for tailoring the mechanical behavior of nc metals via nanostructural stability.

The notion that the motion of low-angle boundaries is coupled to the applied shear stresses is widely accepted^[12] and usually interpreted in terms of the collective motion of the discrete dislocations that comprise the interface.^[13] Extensions of this coupling to high-angle boundaries have been elusive, due in part to the inability to directly observe and model the high-density dislocation content that defines the boundary.^[14] Nevertheless, experimental observations of stress-induced normal GB motion have been reported for Al bicrystals with both low- and high-angle tilt boundaries.^[15] More recently, a universal theory of the coupling phenomenon has been proposed,^[16] wherein ideal coupling of motion within the GB plane (shear strain) to normal motion of the boundary is described by a coupling factor, β , that depends on misorientation angle and temperature and ranges from -1 to 1 . Molecular dynamics (MD) simulations have been used to illustrate the normal migration of flat low and high angle $\langle 001 \rangle$ symmetric tilt boundaries in Cu^[16,17] and $\langle 110 \rangle$ Al GBs,^[17] and also of grain rotation associated with the motion of curved GBs.^[18] GB migration has also recently been observed as a result of applied stress in simulations of polycrystalline systems with more general boundaries.^[3f,19]

In addition to highlighting the role of stress-assisted grain growth in nc-metals, the recent experimental observations of

[*] Prof. K. J. Hemker, Dr. D. S. Gianola,^[+] Dr. C. Eberl^[+]
Department of Mechanical Engineering
Johns Hopkins University
Baltimore, MD 21218 (USA)
E-mail: hemker@jhu.edu

Dr. X. M. Cheng
Advanced Photon Source
Argonne National Laboratory
Argonne, IL 60493 (USA)

[+] Present address: Institute for Materials Research II, Forschungszentrum Karlsruhe, Karlsruhe, Germany.

[**] This work was supported by an NSF NIRT Program (Grant No. DMR-0210215). We thank Prof. Chia-Ling Chien for generously allowing the use of the AFM facility and Dr. Budhika Mendis for valuable comments and discussion.

nanostructural evolution^[5–10] offer a unique opportunity to extend investigation of the Cahn and Taylor unified coupling theory^[16a] to a more general population of GBs. The coupled shear motion of two grains and the migration of their common boundary naturally results in parallelepiped-shaped grains. The manifestation of this process in thin films with threading vertical boundaries should result in the tilting and terracing of individual grains and increased surface roughness. The coupling mechanism implicitly predicts surface relief in thin film geometries with migrating GB planes, as shown schematically in Figure 1a. In the later stages of grain growth, where grain size exceeds the film thickness, lateral GB migration will directly couple to the tangential shearing of individual grains (the angle determined by crystallography and the coupling factor, β), as hypothesized by Cahn et al.^[16a] The coupling theory also directly predicts relative rotation between adjacent grains when any portion of a GB segment is curved (Fig. 1b).^[16a] The expectation of terracing, tilting, and rotation of grains in films undergoing stress-assisted GB migration has motivated the experiments presented here.

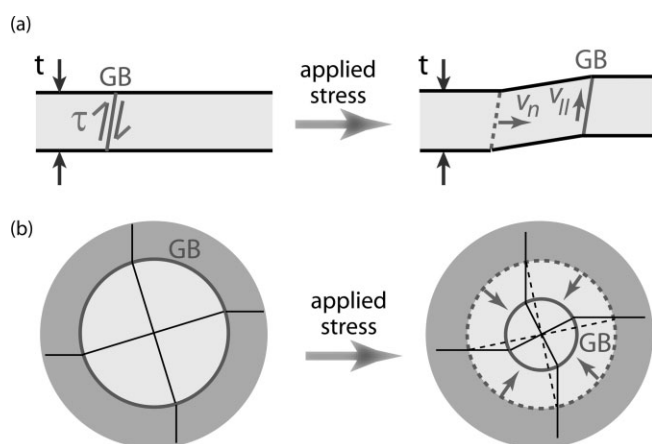


Figure 1. Schematics of shear coupled GB motion after Cahn et al. [16a]. a) Motion of a straight GB is accompanied by shear along the boundary, which leads to surface relief in thin film. b) Motion of a curved boundary leads to grain rotation, as can be seen by considering the growth or shrinkage of an included grain. Orthogonal traces show the misorientation that develops.

In the current study, we employ a sub-micrometer free-standing thin-film geometry to isolate the mechanism responsible for nanostructural evolution in nc Al films. Sputter-deposited nc Al thin film ($150 < t < 300$ nm) microtensile specimens were fabricated using the MEMS-based process flow described earlier.^[5,20] Combining tensile testing of these films with atomic force microscopy (AFM) has allowed us to attribute the ensuing surface topography to local GB events, namely stress-induced shear coupling.

The mechanical behaviors described previously were measured in the current study, and representative tensile responses of freestanding Al thin films are shown in Figure 2. A curve of type-I behavior is shown in Figure 2; these specimens exhibited high strength (15–20 times higher than the strength

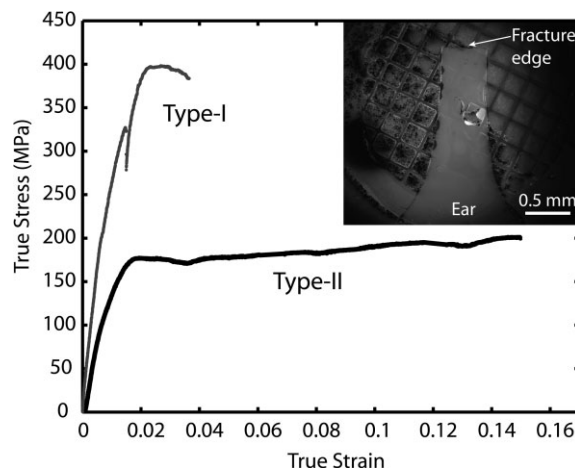


Figure 2. Representative stress strain behavior of Al thin-film specimens showing two distinct types of deformation behavior associated with either a stable microstructure (strong but low ductility) or that of undergoing stress-coupled grain growth (intermediate strength with large total elongations). Inset: a fractured thin film specimen on a Cu grid.

of coarse-grained pure aluminum^[21]) but limited ductility, and are representative of films that maintained a stable nanostructure during deformation. By contrast, type-II specimens (Fig. 2) showed moderate strength and a large elongation to failure. The latter behavior is associated with a specimen undergoing stress-assisted discontinuous grain growth during the course of tensile deformation.^[5]

Scanning electron microscopy (dual-beam SEM/FIB, Nova 600 FEI) was used to characterize the surface relief of these films both before and after deformation. Trenches were cut through the thickness of the film using a focused ion beam (FIB) operating at 30 kV and a beam current of 30 pA. The purpose of these trenches was to observe any variation of thickness or cross-sectional morphology and to provide fiducial markers for subsequent quantification of surface relief using an atomic force microscope.

Images of deformed specimens that underwent extensive stress-assisted grain growth and exhibited extended plasticity (type-II behavior) are shown in Figure 3. Observations made in the ear of the specimen, where stresses were relatively low and where grain growth did not occur showed very little roughness (Fig. 3a). The surface roughness in the ear was the same as as-deposited specimens. By contrast, obvious and widespread surface relief was observed in the gage section of the specimens where grain growth had occurred (Fig. 3b). The degree and magnitude of the surface roughness appeared to scale with the degree of plastic deformation and grain growth.

Parallel experiments were conducted on films that demonstrated the type-I response often reported for nanocrystalline metals: high strength and low ductility with a microstructure that remains static during deformation. The surfaces imaged in these films do not appear to have been affected by the applied load; the surface roughness is the same as was observed on as-deposited material. These observations indicate that the surface relief is correlated with the occurrence of stress-assisted grain growth.

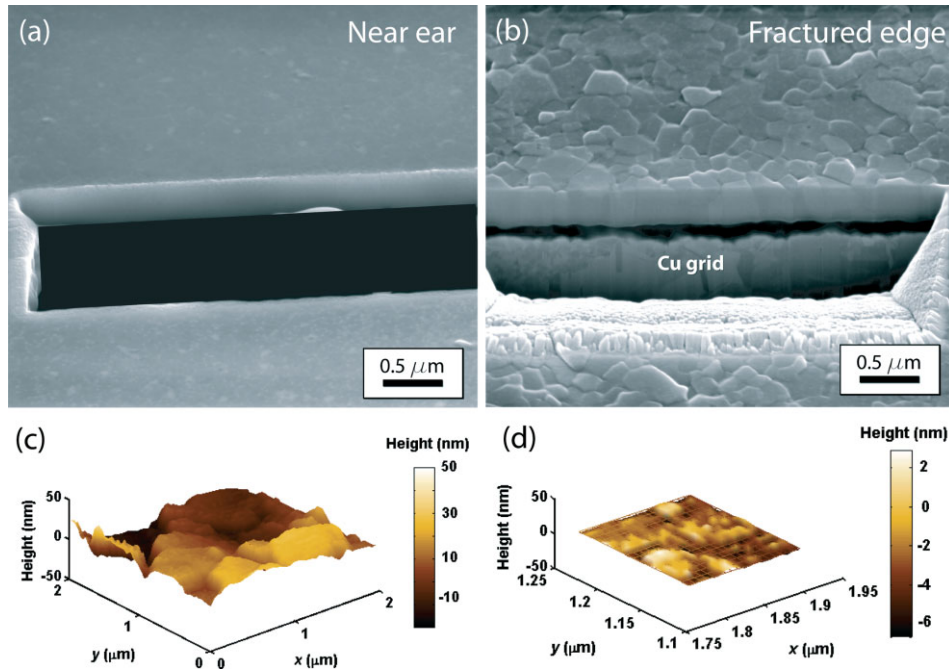


Figure 3. SEM images of nc-Al specimens. a) Surface near ear, and b) surface near fracture edge. AFM images c) evolved surface near fracture edge and d) of grain interior.

AFM operated in tapping mode, was employed to obtain a quantitative assessment of the surface relief. Figure 3c shows a representative AFM scan demonstrating the height profiles obtained near the fracture edge of a specimen that had undergone stress-assisted grain growth. The surface relief is concentrated at the GBs, while the interior of the grains are relatively flat (Fig. 3d) with roughness on the order of the as-deposited material. These measurements also show that the grains have not only shifted vertically, but are also inclined with respect to their neighbors. This observed terracing and grain-level tilting is in agreement with predictions of the stress-coupled GB migration theory put forth by Cahn and colleagues.^[16] The vertical terracing of the grains appears to arise from the shear that is coupled to the normal motion of the boundary, and the grain tilting from coupling on a curved boundary. The shear associated with motion of a curved boundary also leads to rotation of the grains; see for example the schematic of an embedded grain in Figure 1b.^[16a] GB terracing was especially prominent in AFM scans taken near the fractured end of the specimen. Here, it is clear that GBs have not only shifted out-of-plane but also left a sheared region along the surface of the film. The fact that these terraces did not exhibit any systematic orientation and were independent of scan direction discounts the presence of tip artifacts, and indicates that these observations are related to material behavior.

The strain dependence of the surface relief is shown in Figure 4. Strain in the nc-Al thin film specimens was measured

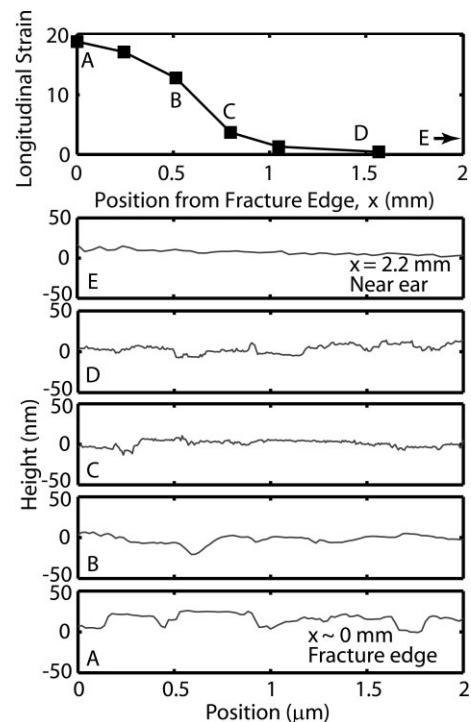


Figure 4. AFM line profiles showing topographical evolution as a function of distance x from the fracture edge. The longitudinal strain gradient from the gage to the ear of the sample is also shown to demonstrate the dependence of topography on deformation. The AFM fast scan direction is perpendicular to the tensile axis.

using custom-developed digital image correlation and tracking software,^[22] and the accumulated plastic strain is shown as a function of position from the fracture edge of a specimen that was pulled to failure. The plastic strain was highest at the point of fracture, fell off away from the fracture surface, and was negligible in the ears of the specimens. AFM line profiles were obtained at various locations along the gage and the surface relief was found to correlate strongly to the applied deformation in the film. The peaks and valleys on the surface correspond to GB locations. AFM topographs were also obtained for a 150 nm thick film that exhibited no grain growth. Observations of various locations on the gage and ear sections of the film confirm SEM observations that no significant change in surface topography occurs.

Standard techniques for quantifying roughness of AFM data^[23] were not sufficient for capturing the topography measured in this work. Typical quantities used for surface roughness include root mean square (RMS) roughness, height-height correlation functions, autocorrelation functions, and power spectral density functions (as has been reported earlier^[25]). While these quantities can be used to describe random roughness, they do not wholly explain the distinctive surface topography evolution uncovered in this study. We have developed a custom analysis algorithm that captures local height information by fitting a plane to the user-selected grain interiors and outputting the surface step height and dihedral angle between two grains along a specified GB. The roughness of the grain interiors was assumed to be negligible based on measurements that show the intragranular roughness of deformed samples ($r_{\text{RMS}} = 2.5$ nm) to be similar to that of as-deposited samples ($r_{\text{RMS}} = 2.6$ nm).

The GB step heights and dihedral angle between adjacent grains of a 300 nm sample that underwent stress-assisted grain growth are plotted in Figure 5. These distributions are plotted in the form of cumulative distribution functions, where the ordinate represents the probability of adjacent grains having a measured value (step height or dihedral angle) that is less than a given value. Near the fracture edge ($x \approx 0$), the values of the step height and dihedral angle are the highest, and gen-

erally decrease as you move toward the ear region of the specimen. A significant difference between the step heights at $x = 0.4$ and 0.7 mm is evident from the change in slope and mean value ($\langle h \rangle_{50}$) of the distribution, while the angle of tilting was similar for these positions. The relief gives rise to individual GB steps that are as large as ca. 60 nm, which is nearly a shift of one entire originally-sized grain, and tilt angles as high as 20° . The mean values for step heights and dihedral angles are 17 nm and 6° at the fractured edge.

It should be noted that the step heights measured on these films are larger than surface relief predicted by thermal- or surface-diffusion-driven GB grooving at room temperature.^[25] Moreover, the presence of a dense native oxide on Al would severely limit the surface diffusion that is necessary for the formation of these grooves, and thermal grooving does not predict rotation or steps between adjacent grains. Surface roughening of unconstrained surfaces of polycrystalline metals undergoing sheet forming processes is also a well-known phenomenon (described earlier^[26]), but this mechanism cannot be used to describe the nc surface roughening uncovered in this study. In conventional surface roughening, the surface perturbations arise as a result of heterogeneous deformation, produced by the accumulation of crystallographic slip events associated with microcrystalline deformation. This would cause intense slip line formation and would be noticeable on the surfaces of the grain interiors. By contrast, the terracing at GBs and tilting observed in these nc-Al films are fundamentally different. Thus, the roughness revealed in this study cannot be associated with plastic deformation-induced surface topography akin to that experienced during metallic sheet rolling and extrusion processes.

The observations of surface topography evolution along with measurements of surface relief have led us to conclude that this phenomenon is directly linked to the occurrence of stress-driven grain growth. The full strain state in the specimen during deformation may also provide some insight to the underpinning deformation mechanisms giving rise to the surface relief. If grain growth is a mechanism for generating plastic strain without the need for dislocation slip events, then the

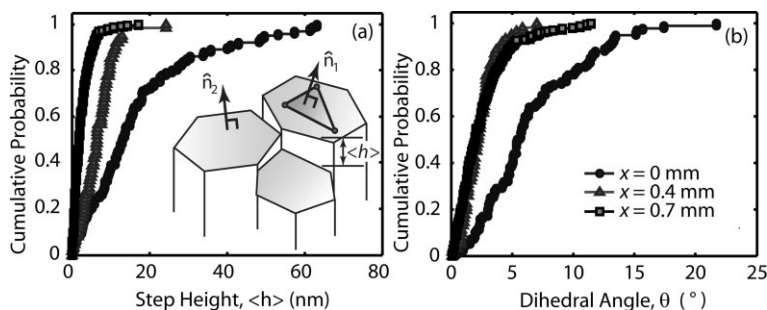


Figure 5. Cumulative distribution functions of a) step heights at grain boundaries, and b) dihedral angles between adjacent grains for a sample that exhibited stress-driven grain growth during tensile testing. The Inset in (a) shows a schematic illustrating the measured quantities, where the dihedral angle, θ , between two adjacent grains is given by $\cos \theta = \hat{n}_1 \cdot \hat{n}_2$. Different data sets correspond to AFM images taken at different distances, x , from the fracture edge ($x = 0$) of the sample.

complete strain (and stress) state for differing degrees of grain growth should be fundamentally different. This hypothesis will now be explored. The strain in the specimen immediately before failure was measured using image correlation, which allowed for the 2D measurement of strain including the longitudinal and transverse stretch components as a function of the position from the fracture edge (Fig. 6). The third component of strain in the thickness direction was determined using SEM images of FIB-cut trenches. Absolute values of the thickness have a considerable uncertainty, so relative measurements using the ear region (no deformation) as the reference were made.

The triaxial state of strain was measured as a function of position from the fracture edge (Fig. 6). Deformation prior to fracture was highly

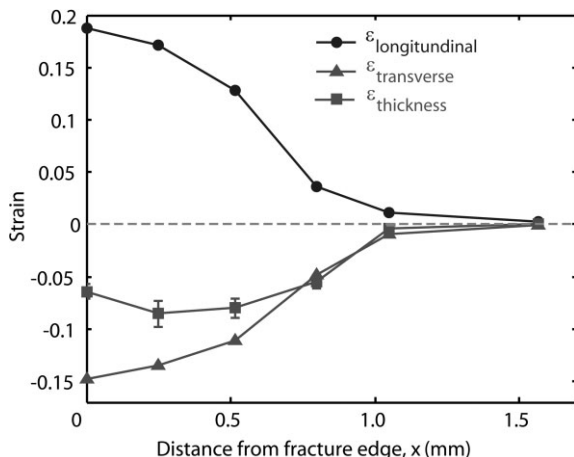


Figure 6. Measured triaxial strain state for a 300 nm specimen just prior to fracture. The longitudinal and transverse strains were measured using our image-based strain measurement, while the thickness strain was estimated from SEM images of cross-sections formed by FIB milling.

localized in the central portion of the gage. The longitudinal and transverse strains both increased monotonically as one gets closer to the fracture edge, while the thickness strain saturated in a manner that suggests that there is a limit to the amount of thickness strain that the specimen can tolerate. It should be noted that the investigated site at $x \approx 0$ was sufficiently far away from any locally thinned region adjacent to the crack, the size of which would be expected to scale with the film thickness. These measurements are consistent with the idea that strain in these nc-specimens is accommodated by stress-assisted GB migration, with the caveat that this mechanism is extinguished once the grains have grown to span the thickness of the specimen. At this point, changes in thickness would have to be accommodated by crystallographic slip or diffusional processes, both of which appear to be more difficult than GB migration.

Taken as a whole, the results of the current study may be summarized as follows: the surface relief and mechanical behavior associated with tensile deformation of nc-Al thin films provide convincing evidence of stress-coupled GB migration as an active deformation mechanism in this class of materials. The importance of stress-coupled boundary migration has been largely overlooked by the materials science community, but when manifest in nc metals the ensuing grain growth produces a dramatic and unmistakable change in properties. It is important to note that the stability and mechanical response of nc-metals is not only different than for coarse-grain counterparts but dynamic as well. The nature and magnitude of the surface relief measured in this study cannot be explained by traditional micro-crystalline deformation mechanisms but are in good agreement with predictions of stress-coupled grain boundary migration and do offer a more general application of Cahn and Taylor's unified theory of GB migration in nc-metals.^[16a]

Experimental

Sub-micrometer thin films were sputtered using a 99.999% pure Al target and structures for performing tensile testing of freestanding films were constructed using standard Si-based microfabrication techniques. The films studied are from the same processing batch as reported earlier [19]; details regarding the film deposition, structure micromachining, and tensile testing apparatus can be found elsewhere [5,21]. Films with nominal thicknesses of 150 and 300 nm were deposited with mean grain sizes of 50 and 100 nm, respectively, as obtained from plan-view TEM measurements. Films were loaded using a displacement-controlled modality where the samples are strained at a rate of $5 \times 10^{-5} \text{ s}^{-1}$.

AFM measurements were conducted using a Veeco Multimode scanning probe microscope operating in AFM tapping mode. The AFM tip length was 125 μm and the resonant frequency was 300 kHz.

Received: July 4, 2007

Revised: September 11, 2007

Published online: January 3, 2008

- [1] a) J. A. Haber, W. E. Buhro, *J. Am. Chem. Soc.* **1998**, *120*, 10847. b) V. Y. Gertsman, R. Birringer, *Scr. Metall. Mater.* **1994**, *30*, 577.
- [2] B. Guenther, A. Kumpmann, H. Kunze, *Scr. Metall. Mater.* **1992**, *27*, 833.
- [3] a) R. Mitra, T. Ungar, T. Morita, P. G. Sanders, J. R. Weertman, in *Advanced Materials for the 21st Century* (Eds: Y. W. Chung, D. C. Dunand, P. K. Liaw, G. B. Olson), The Minerals, Metals & Materials Society, Warrendale, PA **1999**, 553. b) J. Weissmuller, W. Krauss, T. Haubold, R. Birringer, H. Gleiter, *Nanostruct. Mater.* **1992**, *1*, 439. c) T. R. Malow, C. C. Koch, *Mater. Sci. Forum* **1996**, 225-227, 595. d) C. Suryanarayana, C. C. Koch, *Hyperfine Interact.* **2000**, *130*, 5. e) A. J. Haslam, S. R. Phillpot, D. Wolf, D. Moldovan, H. Gleiter, *Mater. Sci. Eng. A* **2001**, *318*, 293. f) A. J. Haslam, D. Moldovan, V. Yamakov, D. Wolf, S. R. Phillpot, H. Gleiter, *Acta Mater.* **2003**, *51*, 2097. g) L. A. Zepeda-Ruiz, G. H. Gilmer, B. Sadigh, A. Caro, T. Ooppelstrup, A. V. Hamza, *Appl. Phys. Lett.* **2005**, *87*, 231904. h) P. C. Millett, R. P. Selvam, A. Saxena, *Acta Mater.* **2006**, *54*, 297.
- [4] a) H. Gleiter, *Prog. Mater. Sci.* **1989**, *33*, 223. b) M. W. Chen, E. Ma, K. J. Hemker, in *Nanomaterials Handbook* (Ed: Y. Gogotsi), CRC Press, Boca Raton, FL **2006**, 497. c) K. S. Kumar, H. Van Swygenhoven, S. Suresh, *Acta Mater.* **2003**, *51*, 5743. d) C. Suryanarayana, *Int. Mater. Rev.* **1995**, *40*, 41. e) H. Van Swygenhoven, J. R. Weertman, *Mater. Today* **2006**, *9*, 24. f) T. Hanlon, Y. Kwon, S. Suresh, *Scripta Mater.* **2003**, *49*, 675. g) T. Hanlon, E. D. Tabachnikova, S. Suresh, *Int. J. Fatigue* **2005**, *27*, 1147.
- [5] a) D. S. Gianola, S. Van Petegem, M. Legros, S. Brandstetter, H. Van Swygenhoven, K. J. Hemker, *Acta Mater.* **2006**, *54*, 2253. b) D. S. Gianola, D. H. Warner, J. F. Molinari, K. J. Hemker, *Scripta Mater.* **2006**, *55*, 649.
- [6] a) K. Zhang, J. R. Weertman, J. A. Eastman, *Appl. Phys. Lett.* **2004**, *85*, 5197. b) K. Zhang, J. R. Weertman, J. A. Eastman, *Appl. Phys. Lett.* **2005**, *87*, 1.
- [7] G. J. Fan, L. F. Fu, D. C. Qiao, H. Choo, P. K. Liaw, N. D. Browning, *Scripta Mater.* **2006**, *54*, 2137.
- [8] R. Schwaiger, personal communication.
- [9] G. J. Fan, Y. D. Wang, L. F. Fu, H. Choo, P. K. Liaw, Y. Ren, N. D. Browning, *Appl. Phys. Lett.* **2006**, *88*.
- [10] a) M. Jin, A. M. Minor, E. A. Stach, J. W. Morris, Jr., *Acta Mater.* **2004**, *52*, 5381. b) J. W. Morris, Jr., M. Jin, A. M. Minor, *Mater. Sci. Eng. A* **2007**, *462*, 412. c) Z. Shan, E. A. Stach, J. M. K. Wiezorek, J. A. Knapp, D. M. Follstaedt, S. X. Mao, *Science* **2004**, *305*, 654.
- [11] D. S. Gianola, B. G. Mendis, X. M. Cheng, K. J. Hemker, *Mater. Sci. Eng. A*, DOI: 10.1016/j.msea.2006.12.155.

- [12] a) C. H. Li, E. H. Edwards, J. Washburn, E. R. Parker, *Acta Metall.* **1953**, *1*, 223. b) D. W. Bainbridge, C. H. Li, E. H. Edwards, *Acta Metall.* **1954**, *2*, 322.
- [13] W. T. Read, W. Shockley, *Phys. Rev.* **1950**, *78*, 275.
- [14] J. C. M. Li, *Phys. Rev. Lett.* **2006**, 96.
- [15] a) M. Winning, G. Gottstein, L. S. Shvindlerman, *Acta Mater.* **2001**, *49*, 211. b) M. Winning, G. Gottstein, L. S. Shvindlerman, *Acta Mater.* **2002**, *50*, 353. c) M. Winning, *Z Metallkd.* **2005**, *96*, 465. d) M. Winning, A. D. Rollett, *Acta Mater.* **2005**, *53*, 2901.
- [16] a) J. W. Cahn, J. E. Taylor, *Acta Mater.* **2004**, *52*, 4887. b) J. W. Cahn, Y. Mishin, A. Suzuki, *Philos. Mag.* **2006**, *86*, 3965. c) J. W. Cahn, Y. Mishin, A. Suzuki, *Acta Mater.* **2006**, *54*, 4953.
- [17] Sansoz, J. F. Molinari, *Acta Mater.* **2005**, *53*, 1931.
- [18] a) J. Haslam, D. Moldovan, S. R. Phillpot, D. Wolf, H. Gleiter, *Comput. Mater. Sci.* **2002**, *23*, 15. b) M. Upmanyu, D. J. Srolovitz, A. E. Lobkovsky, J. A. Warren, W. C. Carter, *Acta Mater.* **2006**, *54*, 1707. c) S. G. Srinivasan, J. W. Cahn, in *Science and Technology of Interfaces* (Eds: S. Ankem, C. S. Pande, I. Ovidko, R. Ranganathan), TMS, Seattle, WA **2002**, 3.
- [19] a) Sansoz, V. Dupont, *Appl. Phys. Lett.* **2006**, 89. b) D. Farkas, A. Froseth, H. Van Swygenhoven, *Scripta Mater.* **2006**, *55*, 695. c) J. Monk, D. Farkas, *Phys. Rev. B* **2007**, 75.
- [20] D. Gianola, K. Hemker, M. Legros, W. Sharpe, Jr., *TMS Lett.* **2004**, *1*, 149.
- [21] J. R. Davis, *ASM Specialty Handbook: Aluminum and Aluminum Alloys*, ASM International, Metals Park, OH **1993**.
- [22] a) C. Eberl, R. Thompson, D. S. Gianola, W. N. Sharpe, Jr., K. J. Hemker, *MATLAB File Exchange* **2006**, www.mathworks.com (accessed October 2007). b) W. N. Sharpe, Jr., J. Pulskamp, D. S. Gianola, C. Eberl, R. Polawich, R. Thompson, *Exp. Mech.* **2007**, *47*, 649.
- [23] a) Majumdar, B. Bhushan, *J. Tribol. Trans. ASME* **1990**, *112*, 205. b) J. Ruan, B. Bhushan, *J. Tribol. Trans. ASME* **1994**, *116*, 378. c) B. Bhushan, B. K. Gupta, M. H. Azarian, *Wear* **1995**, *181–183*, 743.
- [24] Rasigni, F. Varnier, M. Rasigni, J. P. Palmari, A. Llebaria, *Phys. Rev. B* **1983**, *27*, 819.
- [25] W. W. Mullins, *J. Appl. Phys.* **1957**, *28*, 333.
- [26] a) Y. Z. Dai, F. P. Chiang, *Mech. Mater.* **1992**, *13*, 55. b) W. Tong, L. G. Hector, Jr., H. Weiland, L. F. Wieserman, *Scripta Mater.* **1997**, *36*, 1339. c) Y. S. Choi, H. R. Piehler, A. D. Rollett, *Metall. Mat. Trans. A* **2004**, *35 A*, 513. d) Z. Zhao, R. Radovitzky, A. Cuitino, *Acta Mater.* **2004**, *52*, 5791.